

On-orbit performance of the double delay line detectors for the *Far Ultraviolet Spectroscopic Explorer*

David J. Sahnou^{*a}, Mark A. Gummin^b, Geoffrey A. Gaines^c, Alex W. Fullerton^{a,d}, Mary Elizabeth Kaiser^a, Oswald H. W. Siegmund^c

^a Department of Physics and Astronomy, The Johns Hopkins University, Baltimore, MD 21218

^b MAG Systems, 1731 St. Andrews Court, St. Helena, CA 94574

^c Space Sciences Laboratory, University of California, Berkeley, CA 94720

^d Department of Physics and Astronomy, University of Victoria, Victoria, BC V8W 3P6

ABSTRACT

The *Far Ultraviolet Spectroscopic Explorer* (FUSE) satellite was launched into orbit on June 24, 1999. FUSE is designed to make high resolution ($\lambda/\Delta\lambda = 20,000 - 25,000$) observations of solar system, galactic, and extragalactic targets in the far ultraviolet wavelength region (905 - 1187 Å). Its high effective area, low background and planned three year life allow observations of objects which have been too faint for previous high resolution instruments in this wavelength range.

The FUSE instrument includes two large format microchannel plate detectors. Each detector system consists of two microchannel plate segments in a Z-stack configuration with double delay line anodes and associated electronics. High detector spatial resolution was required in order to obtain scientific data with high spectral resolving power, and low detector background was necessary in order to observe faint objects.

We describe the performance of the FUSE detectors during their first year on orbit, including the mechanical and thermal stability, throughput, background, and flat field of the detector system. We will also discuss the regular single event upsets of the detector electronics, and the strategy adopted in order to minimize their impact on mission efficiency.

Keywords: FUSE, microchannel plates, spectroscopy, ultraviolet, delay line

1. INTRODUCTION

The *Far Ultraviolet Spectroscopic Explorer* (FUSE), was designed to obtain high resolution spectra of astrophysical objects in the far ultraviolet wavelength region (905 - 1187 Å) in order to investigate a large number of scientific problems.¹ The scientific objectives of FUSE require high both high spectral resolving power and high sensitivity, to determine elemental abundances along lines of sight in the Milky Way galaxy and in other galaxies. FUSE was launched into a low earth orbit on a Delta 2 ELV from Cape Canaveral Air Station on June 24, 1999. It is designed to have a three year mission lifetime.

This paper describes the performance of the two FUSE detectors during their first year on orbit. Information from prelaunch tests will also be included, as appropriate. An earlier paper² described the planned design of the detectors and their performance based on flight prototype units; this work will describe the calibration and use of the actual flight units and the flight spare.

1.1. FUSE design

The FUSE instrument consists of four coaligned channels, each consisting of an off-axis parabola primary mirror, a Focal Plane Assembly containing the spectrograph entrance apertures, an aberration-corrected holographic grating in a Rowland circle mount, and one half of a detector. The optics on two of the channels are coated with silicon carbide (SiC), in order to provided reflectivity across the entire FUSE bandpass; the other two are coated with lithium fluoride

* Correspondence: Email: sahnou@pha.jhu.edu; Telephone: 410 516 8503; Fax: 410 516 5494

(LiF) over Aluminum in order to provide the highest reflectivity above 1150 Å. Details of the design have been given elsewhere.³

1.2. Primary performance requirements

The resolution ($\lambda/\Delta\lambda = 20,000 - 25,000$), throughput and wavelength coverage (905 - 1187 Å) requirements of the FUSE mission, combined with the packaging constraints due to the Delta 2 fairing, resulted in the requirements for a large format detector with high spatial resolution which was curved to match the spectrograph Rowland circle. Although the holographic corrections on the gratings reduce the astigmatism of the system substantially from that of a standard Rowland design, the remaining astigmatism, coupled with the requirement of multiple entrance apertures, led to a requirement for two-dimensional detectors in order to collect all the light from a target. The astigmatic height of each spectrum can be nearly 1 mm tall; this height, coupled with the requirement that light from the three apertures not overlap, requires an active area of approximately 4 mm in the cross dispersion direction. The decision to put the spectra from two channels on the same detector and leave room for possible misalignments between them led to a requirement for a 10 mm active area in that axis.

In order to resolve spectral lines that are only separated by 1 part in 20,000 or less, the detector must have an intrinsic resolution on the order of 20 μm in the dispersion direction. The y resolution is much less of a concern because of the astigmatic height of the spectra, although the curvature of the spectra and desire not to have light from adjacent slits overlap does result in a requirement of ~100 μm or better.

For maximum simultaneous wavelength coverage, the longest possible detector was desired. Since the dispersion of the gratings is on the order of 1 Å/mm, a nearly 300 mm long detector would be necessary to cover the full spectral range. Requiring that only 2 of 4 channels be active at each wavelength led to a requirement for a length of just under 200 mm. Since microchannel plates (MCPs) and anodes that long were impractical, a gap was allowed on each detector, so that it could be divided into two independent segments. To minimize the loss of wavelength coverage, the size of this gap was limited to be less than 10 mm.

2. DETECTOR SYSTEM DESIGN

The detectors designed to meet the requirements discussed above are microchannel plate detectors with helical double delay line anodes. This design builds upon previous UC Berkeley designs used on other space missions, such as EUVE,⁴ ORFEUS,⁵ and SOHO.⁶ In addition, the far ultraviolet detector in the Cosmic Origins Spectrograph⁷ for the Hubble Space Telescope will be very similar to the FUSE detectors, and shares much of the same mechanical design. All of these detector systems share some of the FUSE characteristics, but each design is unique due to the different mission requirements. This section will describe the details of the FUSE detector design.

The detector subsystem includes two identical detectors, each containing two independent segments. Mechanically, each detector is a single unit; electrically, however, each segment is unique, with most of its own electronics. An accompanying overview paper⁸ provides details of how the detector fits in to the overall instrument layout, and how the spectra fall on the detector.

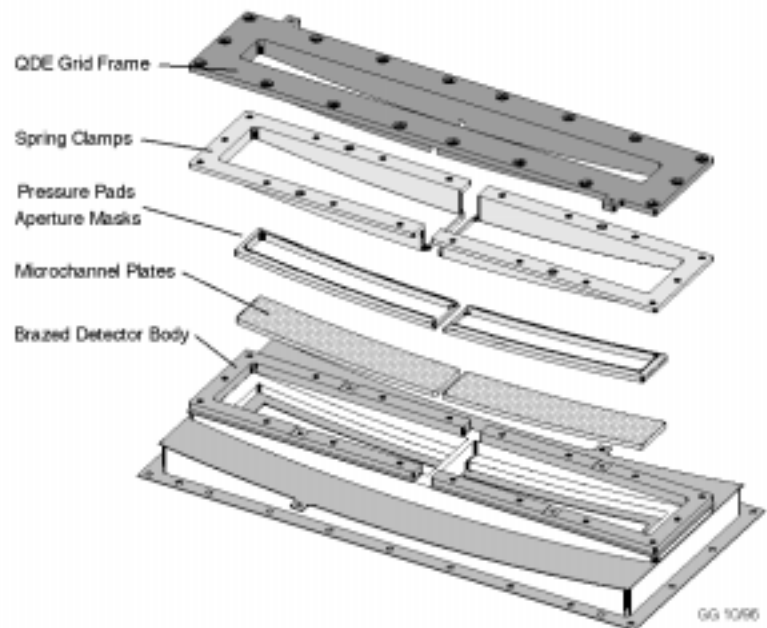


Figure 1 Detector body assembly.

The two segments in each detector are contained in a single vacuum housing. To ensure the highest resolution across the entire band, the two segments are mounted along a single, machined surface; this allows the front surface of the MCPs to match the cylindrical 1652 mm diameter Rowland circle to within $\sim 25 \mu\text{m}$. A schematic of the detector body assembly is shown in figure 1. Each segment consists of a Z-stack of $95 \times 20 \text{ mm}$ microchannel plates with 13° bias angles. Details of the MCPs for the two detectors are shown in Table 1. The front and back MCP have different pore sizes and spacings from the middle plate in order to minimize the moiré pattern which is often seen when identical MCPs are stacked.⁹ The front plate of each segment is coated with an opaque KBr photocathode in order to increase the quantum efficiency in the far ultraviolet. The top MCP is held at a voltage of ~ 4600 volts, depending on the segment.

7 mm behind each MCP stack is a helical double delay line (DDL) anode, with an active area of $94 \times 20 \text{ mm}$. The anode, constructed on a flexible RT/Duroid substrate, is curved to match the MCP shape. The anode period is $600 \mu\text{m}$, and the anode-MCP voltage difference is 550 volts.

In front of the MCPs are two 95% transmission nickel mesh screens. The first is the “QDE grid,” which is curved to match the surface of the front MCP, and is located 6 mm from that surface; its purpose is to increase the quantum detection efficiency of the detector, by forcing photoelectrons generated on the MCP web down the pores. This grid is held at 1200 volts above the front MCP. Also included

in the design is a flat, “Plasma grid” (not shown in the diagram) which is held at +15 volts, and is mounted across the detector aperture on the inside of the vacuum box, approximately 35 mm from the MCPs. This is used to keep charged particles from reaching the detector and possibly increasing the background.

The detector body assembly is bolted to a stainless steel backplate, which provides the mechanical and thermal interface to the rest of the instrument. Also mounted to the backplate is a mu-metal magnetic shield, which surrounds the body assembly and shields the detector from stray magnetic fields, which may cause image motion. This entire assembly is enclosed inside a vacuum box, which protects the photocathode from ambient atmosphere, and permitted high voltage operation when the instrument was at normal atmospheric pressure; two 4 l/s ion pumps on each detector were used to maintain a low enough pressure ($< 10^{-6}$ torr) so that high voltage could be operated on the ground during integration and test. A mechanical door with a sapphire window in front of each segment allowed illumination at ambient pressure. During vacuum testing on the ground, the door was opened in order to allow illumination with ultraviolet light. Once on orbit, the doors were opened one final time.

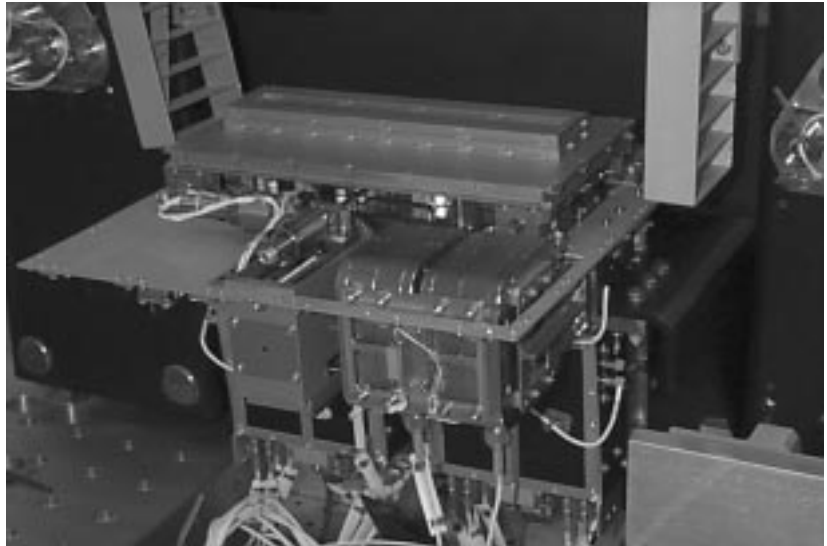


Figure 2 Detector installed in the spectrograph cavity.

Mounted to the backplate are two high voltage filter modules, which supply the voltage required for the MCPs, the QDE grids, and the rear field between the back MCP and the anode. The backplate also supports the amplifiers, which provide the gain necessary for the electronics to be able to process the pulses from the anode. Figure 2 shows a photo of a detector just after it was installed in the spectrograph. The detector door is at the top, with its protruding rectangular light baffle. In the front right are the two ion pumps. The amplifiers and filter modules are visible behind the pumps.

Table 1 MCP Characteristics

Detector	Segment	Plate	Manufacturer	Pore Size	Pore Spacing	S/N
Detector 1 (S/N FL02)	A	Top	Philips	10	12.5	ML201-A-1-6
		Middle	Philips	12.5	15	KK502-C-26
		Bottom	Galileo	10	12.5	96M0014-24
	B	Top	Philips	10	12.5	ML201-A-2-5
		Middle	Philips	12.5	15	KK502-C-35
		Bottom	Galileo	10	12.5	96M0014-45
Detector 2 (S/N FL03)	A	Top	Galileo	10	12.5	95M0049-30
		Middle	Philips	12.5	15	KK502-C-31
		Bottom	Philips	10	12.5	BD001-B-36
	B	Top	Galileo	10	12.5	95M0049-33
		Middle	Philips	12.5	15	KK502-C-28
		Bottom	Philips	10	12.5	BD001-A-26

Photons that strike the MCPs create photoelectrons at the photocathode, which are then accelerated through and amplified by the MCPs until a charge cloud several millimeters in size and containing $\sim 10^7$ electrons emerges from the back end and strikes the anode. The DDL uses timing circuitry to locate the x (dispersion direction) centroid of this charge cloud, and a simple charge division algorithm in the y (cross dispersion) direction. A schematic of the pulse location electronics is shown in Figure 3.

Since these detectors do not have fixed size pixels, but rely on analog measurements to determine the location of the incident photons, it is necessary to monitor the overall stretch and shift of the coordinate system. This is done by inserting two stimulation pulses on each segment for 60 seconds at the beginning and end of every exposure. These stim pulses are generated by injecting charge into the amplifiers such that events appear near the right and left edge of the segment beyond the active area of the MCP. Each stim pulse has a fixed rate of

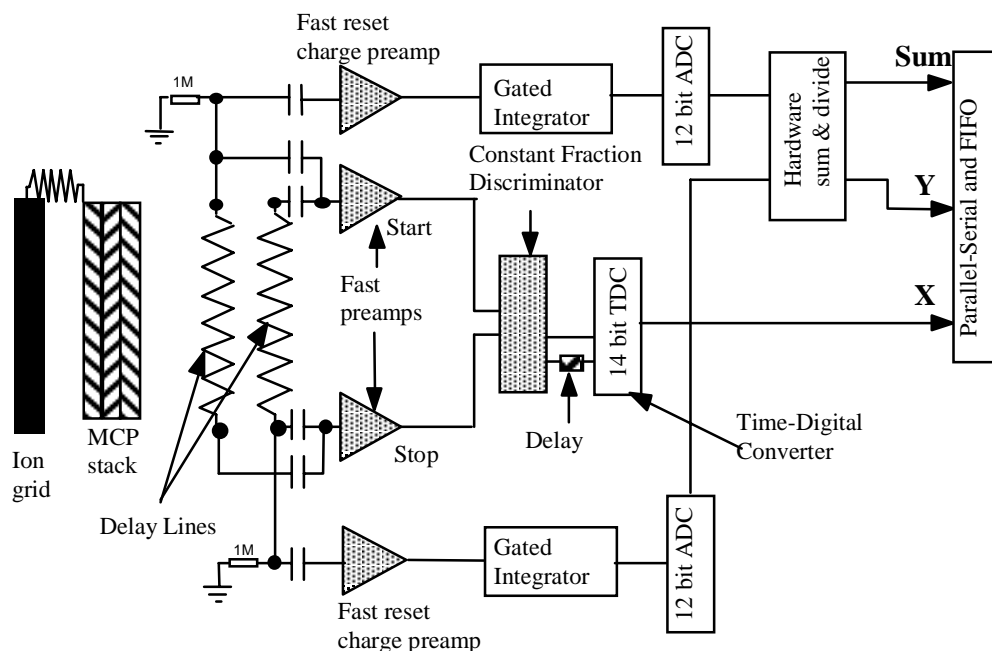


Figure 3 Encoding electronics for the FUSE detector.

approximately 45 counts per second for each. Nominal detector pixel sizes are 5.92 to 5.98 μm in x, and 9.1 to 17.3 μm in y, depending on segment; nonlinearities are typically only a few percent, except at the edges here they are somewhat worse.

The detector Data Processing Unit (DPU) is responsible for the electronic processing of the collected events. At boot up, a control program is loaded into memory from an onboard EPROM. It contains two 32 KB regions from which code may be executed; these are known as the upper core (UC) and lower core (LC) memory. Booting up loads the EPROM version of code into LC. A modified version of this code, with additional detector protection functions, is then loaded into UC, and then the UC code is executed. Early in the mission, UC code could only be loaded from the ground. With modifications to both the Instrument Data System (the instrument computer; IDS) code and DPU code (the latter to allow checking of the CRC to verify the code load was successful), the entire process now occurs autonomously on board. This was an important part of the SEU mitigation strategy (see section 4.3 below). The DPU electronics are located away from the detector head, in the instrument electronics cavity.

In addition to processing the photon positions, the detector DPU performs other important tasks. Five independent user-programmable masks are available, along with a total count monitor. Each of the programmable masks consists of a region of memory, with one bit for each 16×16 pixel region area on the detector. Setting a mask bit to 1 allows processing of a photon that lands in that pixel region; setting it to 0 causes the DPU to discard it. Table 2 lists the masks and their default uses. During a typical observation, the SiC and LiF counters are chosen to only include the light from the slit containing the target, the ASC includes an area of the detector not illuminated by spectra, and the remaining masks are set to include the entire detector area.

Table 2 Detector Counters and Masks

Mnemonic	Name	Use
FEC	Fast Event Counter	Total counts reaching the detector
DEC	Digitized Events Counter	Events above threshold
AIC	Active Image Counter	Counts sent to the IDS
ASC	Autonomous Shutdown Counter	SAA monitoring
SiC	SiC Counter	Peakup in SiC channel
LiF	LiF Counter	Peakup in LiF channel

Each event which is not rejected by the masks is packaged into a 32 bit word, containing a 14 bit x position, a 10 bit y position, 5 bits of pulse height, 2 bits noting the detector and segment, and one bit denoting that this is a valid photon event. This data is then transferred to the IDS via the science data bus. The IDS polls the two detectors, and reads the event at its next opportunity.

The IDS has two separate ways of processing the incoming photon events. The first is time tag (TTAG) mode, in which the 32 bit word for each photon (up to a maximum rate of 8,000 cps from all four segments) is saved for transmission to the ground. At a user-specified interval (with choices from once per second to 125 times per second), a time marker is inserted into the data stream. The availability of the time markers allows the data to be corrected for spectral motion¹⁰ and Doppler shift, while the pulse height can be used to for pulse height screening, in cases where the lowest possible background is desired.

At higher count rates (up to 32,000 cps from all four segments), data is normally saved in histogram (HIST) mode. In this case, the relevant portion of the detector is mapped to a two-dimensional array in memory, and the (x,y) coordinates of each incoming photon are used to increment a memory location. In this way, a two dimensional image of the detector is built up; timing and pulse height information is discarded. Because of memory limitations, this data is typically binned by 8 pixels in y (resulting in a small loss of resolution), and only data from slits containing the target are saved. HIST mode is typically used when the count rates are higher than about ~2500 cps, where the onboard memory needed for a TTAG exposure is likely to be comparable to that needed for a HIST exposure.

The IDS also monitors the FEC, and if its rate exceeds a predefined value (the default is 45,000 cps for a segment), it drops the HV to a safe level in order to protect the MCPs.

The final component of each detector system is the stimulation lamp. Each detector has a mercury penray-type lamp, mounted ~1.5 meters in front of the detector face. The lamp illuminates the detector directly, without any intervening optics; consequently, it does not have the same f-ratio as the illumination from science targets. The stim lamp, which is controlled via the detector DPU, provides a roughly uniform illumination of each segment with the exception of the regions shadowed by the wires from the plasma and QDE grids. Stim lamp exposures are used primarily to monitor long term shifts in the detector format.

3. PREFLIGHT CALIBRATION

After construction was completed, the detector subsystems, consisting of the detector head, DPU, and stim lamp, underwent an extensive series of tests at UC Berkeley. At the conclusion of that testing, the flight detectors were installed in the FUSE spectrograph structure at the University of Colorado, where spectrograph assembly and alignment were carried out. The fully aligned spectrograph was then shipped to the Applied Physics Laboratory in Laurel, MD, where satellite integration and test was done. Finally, a thermal vacuum end-to-end test was completed at the Goddard Space Flight Center, and the entire satellite was shipped to Florida for launch. This section will describe the results of some of the preflight testing, with an emphasis on the testing that relates to the on-orbit performance.

3.1. Quantum Detection Efficiency

The overall sensitivity of the instrument is due primarily to the reflectivities of the mirrors and gratings, and the quantum detection efficiency (QDE) of the detectors. The MCPs were coated with a KBr photocathode in order to maximize the efficiency in the far ultraviolet. After deposition of the photocathode, measurements of the QDE were made at several wavelengths across the FUSE band. Figure 4 shows the results of these measurements. QDE degradation is not expected to be a major factor in loss of efficiency during the mission; instead, loss of reflectivity of the mirror and grating coatings is expected to have a much greater effect.

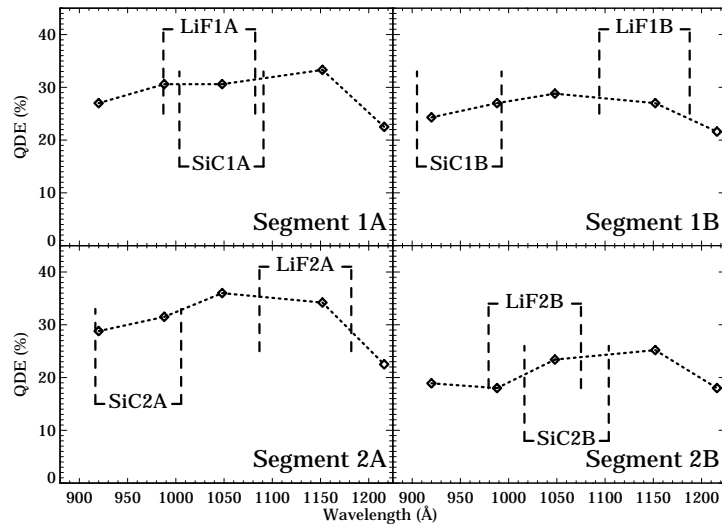


Figure 4 Preflight measurements of QDE for all segments. Also shown is the SiC and LiF wavelength coverage on each segment.

3.2. Detector resolution and distortion

During detector construction and testing, regularly-spaced grids of 10 μm diameter pinholes, spaced 1–2 mm apart, were placed directly on the front MCPs of each segment to measure linearity and resolution. Distortions also exist at higher spatial frequencies, at both the pore and multifiber boundary level. These variations, which are very difficult to map without difficult and time-consuming testing, tend to be washed out in the science data due to the relatively large height of the spectra on the detector. However, they most likely introduce some distortions over very small spatial scales, which will introduce errors in the absolute wavelength scale of the calibrated spectra.

The pinhole data were also used for a preflight resolution determination. The FWHM of each pinhole was measured, and detector settings were modified to maximize resolution over as much of the detector as possible. Typical results showed FWHMs of ~20–25 μm in x, and 80–100 μm in y. No in-flight measurements of resolution are possible, since changes in the intrinsic spectrograph resolution with wavelength mask most of the detector effects.

During spectrograph integration and test, lines from an H_2 lamp were used to illuminate the flight gratings in a manner similar to the flight telescope mirrors. This source provided a high density of lines, which was used to map the detector spatial linearity and wavelength scale on both long (several mm) and short (< 1 mm) spatial scales.¹¹ FUSE carries no onboard wavelength calibration source, thus requiring the use of astronomical sources to determine the wavelength

scale. Because of the difficulty in finding targets with a high density of spectral lines, in addition to problems identifying the absolute wavelength of many of the lines found, this ground-based wavelength scale is still the basis of the on-orbit wavelength scale. Work is underway to improve this solution using primarily astronomical targets.

The distortion appears to be stable, aside from an electronic shift and stretch of the entire format as the temperature changes (see section 4.5).

Tests on the flight spare detector have shown that the shape of the point spread function, and hence the resolution, is a function of count rate.¹² The effect only becomes serious at high count rates (>5000 cps), however. Since typical TTAG count rates are much lower than this, it should have a negligible effect for most FUSE observations. HIST observations, which can have significantly higher count rates, are binned by 8 pixels in y, which degrades the resolution (due to spectral curvature) by 5 – 10%.

3.3. Detector mounting

During installation of each detector, shims were placed between the structure mounting plate and detector backplate in order to match the previously measured MCP location to the Rowland circle. The MCP locations were located to within $\sim 37 \mu\text{m}$ to an optical cube on the backplate. Since the detectors were the first optical element mounted to the structure, it ultimately defined the coordinate system, and the placement of gratings and other optical elements were tied to it; however, due to constraints on the ability to rotate the gratings, the goal was to get the detector rotation correct. During the mounting of detector 1, a 6.3 arcsecond tilt was inadvertently introduced, and schedule constraints did not allow this to be corrected. This tilt results in the inability to perfectly focus both ends of the spectrum simultaneously on that detector. The decision was made to sacrifice some resolution at the lowest wavelengths, where the sensitivity is lowest. On-orbit, changing the position of the FPAs allows temporary improvement in that wavelength region; in practice, the instrument resolving power does not appear to be limited by this effect.

3.4. Current spikes

During the optical end-to-end test at Goddard Space Flight Center, periodic excursions of the detector high voltage current occurred. Although for the most part, these events are of short duration (<40 ms) and thus are not a hazard to the detector, the DPU code was modified to include a threshold for the high voltage current and auxiliary power supply current. If any of the thresholds are exceeded, the DPU issues a diagnostic code, which is reported to the ground. If the threshold is exceeded for a ground-selectable time (currently 20 ms), the high voltage on the affected segment is shut down as a precautionary measure. Telemetry also monitors and records these three values every 1 ms. An operational constraint requires that this version of the DPU code be used whenever detector high voltage is turned on.

4. PERFORMANCE

4.1. Early operations

The electronics for the two detectors were turned on six days after launch, on June 30, 1999. Within several days of turn on, internal detector CRC checking reported an error in the DPU code space memory. During the next day, two more of these memory errors were reported. These were later traced to single event upsets (SEUs), which have had a major impact on detector operations since then (see section 4.3).

After letting the spectrograph cavity partially outgas, the detector doors were opened on July 16 and 17, 1999. Once the doors were opened, the detector ion pumps were used to monitor the pressure in the spectrograph cavity. The pressure reached a low enough value to ramp up high voltage by mid August. On August 13, 1999, high voltage was turned on for detector 1. Detector 2 high voltage was first used on August 26. During the high voltage ramp up of detector 1, the first ‘event burst’ was recorded (see section 4.4).

4.2. Normal Detector Operations

During normal operations, the detector is always on and collecting data; this data is saved and sent to the ground only when the IDS is instructed to take an exposure, however. During a typical observation, data is saved only during the parts of the orbit when the target is not occulted and the satellite is not passing through the South Atlantic Anomaly (SAA). The detector has built-in bright object protection (in addition to the IDS bright object protection discussed above), which lowers the high voltage to a safe level whenever the count rate in the ASC mask exceeds a certain

threshold. However, during normal SAA passages, this is not used in favor of having the IDS lower the voltage via an onboard SAA Manager, which reads a table of SAA ingress and egress times, and lowers the voltage as appropriate. These times are generated by the Mission Planning group, and are the same as those used to plan the beginning and end of exposures.

When an SEU or ground command turns off the high voltage, it now requires a lengthy process (> 12 hours) to return the voltage to its nominal value. This long time is required in order to limit the thermal changes to the MCPs, since they may have been unpowered for many hours by the time the ground-initiated procedure can begin. In addition, due to the fact that a typical 100 minute orbit has at most one ~10 minute ground contact and there is a long blackout period with no ground contacts every day, it can take as long as 24 hours to return to full voltage. The ramp up is now in the process of being automated, in order to dramatically shorten this time. The likelihood of needing this automation was recognized before launch, but it was decided that initially all ramp up operations would be via ground command for maximum safety.

4.3. Single Event Upsets

The only significant detector anomaly discovered on orbit was the sensitivity of the electronics to single event upsets. Soon after the detector electronics were powered on, the DPU began reporting errors in the memory that stores the code controlling the detector. Further investigation revealed that the memory was being corrupted by high energy particles as the satellite passed through the SAA. The SEUs have no effect on the science data, but are a potential detector health and safety issue, since corruption of the executing code could cause unpredictable behavior. When the problem was first discovered, stringent rules were developed which required rebooting the detector if a second SEU occurred before the first could be repaired; this had a major impact on observing efficiency in late 1999. Modifications to the DPU code made in December 1999 included an UC CRC check, and the checking of a smaller memory range in order to avoid responding to bit flips which occur outside of the code regions.

Currently, the SEU rate in code space is about one per detector every 4 days; a total of 210 were seen during the first year of the mission. SEUs also occur in mask memory, where they have the effect of turning on or off a 16×16 pixel region in a mask. A fix is currently being implemented to minimize this effect, also.

Figure 5 shows the orbital locations of all the SEUs obtained during the first year on orbit. As expected, they are concentrated towards the center of the SAA. The orbital inclination of the satellite means that it never dips below -25° latitude, so there is an abrupt cutoff in the SEUs at that position.

4.4. Event bursts

An unexplained phenomenon discovered soon after high voltage turn-on was the occurrence of 'event bursts,' or rapid increases in the count rate. These bursts have durations that range from a few seconds to several hundred seconds, with maximum count rates that can reach 20,000 counts per second. Although the bursts generally happen during orbital morning (often near noon) attempts to correlate their occurrence with orbital location, ram vector, or other orbital circumstances have not been successful.

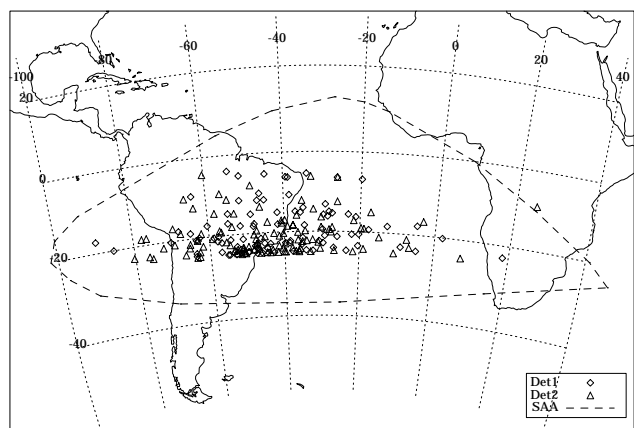


Figure 5 Orbital locations of SEUs since the beginning of the mission.

Figure 6 shows the count-rate associated with a typical FUSE burst as a function of time. Qualitatively similar events have been detected in the microchannel plate detectors on Chandra¹³ and ALEXIS¹⁴. The pulse height distribution of an event burst is consistent with the distribution exhibited by photons, which suggests that the events due to light rather than energetic particles. The spatial distribution of event bursts is quite different from the distribution of spectra, but tends to follow one of a few standard patterns. Often, event bursts cause the grid wires to appear in emission; see, for example, Figure 7.

Early in the mission, bursts would regularly cause the detector SAA protection to trigger. Modifications to the thresholds were implemented in order to keep this from occurring. The incidence of bursts has decreased markedly since the first three months of high voltage operations. This decline in frequency suggests that the pressure in the spectrograph cavity might play a role in producing the bursts.

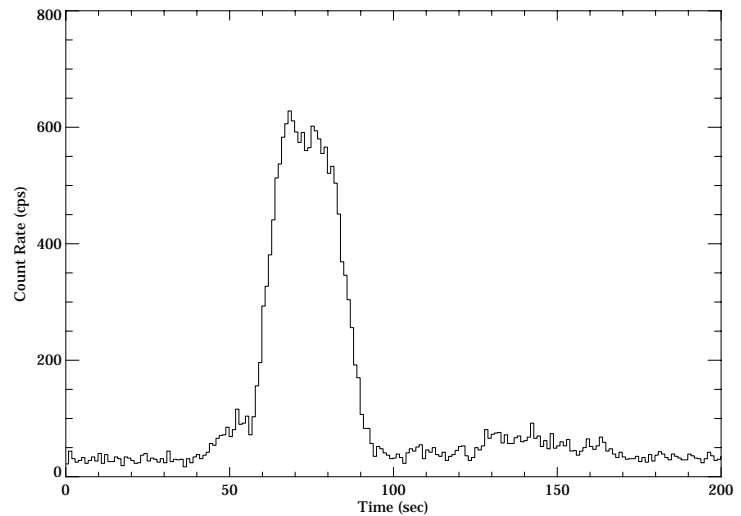


Figure 6 Time profile of a typical event burst.

4.5. Stability

The stability of the pixel coordinate system of each detector segment is routinely monitored through measurements of the positions of the stimulation pulses. Figure 8 summarizes these measurements since launch for detector segment 1B. The upper panel shows the shifts in the mean x-position of the stim pulses with respect to an arbitrary reference frame as a function of time since the initial HV ramp-up. The middle panel shows the difference in x-position of the stim pulses with respect to the same reference frame, which traces the stretches or contractions in the apparent length of the detector. The lower panel shows the temperature of the time-to-digital converter (TDC) for segment 1B. Analogous data for the remaining segments is very similar.

The figure shows that the on-orbit thermal environment of the detectors is very stable. The full range of TDC temperature excursions during routine operations (i.e., after day 85, when the temperature of the spectrograph cavity was changed) is no more than 2° C. Larger variations were exhibited prior to this date, largely because the temperature of the instrument cavity was not being controlled actively.

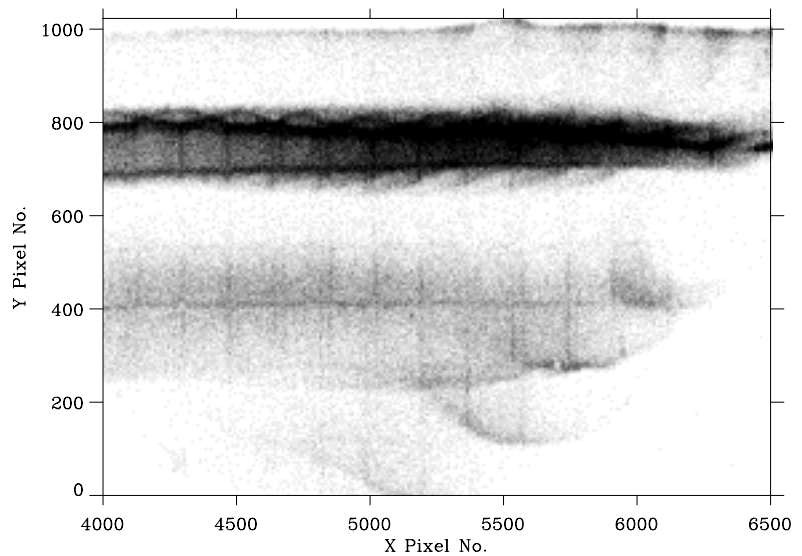


Figure 7 Spatial distribution of a burst on the detector.

As a result of this thermal stability, changes in the apparent metric of the detector are also very small. For extended periods of time, the shifts are on the order of a pixel, with little scatter. Similarly, the stretches are on the order of 2-3

pixels (i.e., fractional changes in the detector length of only $\sim 0.02\%$), with somewhat larger scatter. In general, the shifts and stretches correlate well with the temperature variations exhibited by the TDC, though there are noticeable lags. In addition, there is a long-term trend evident in both the shift and stretch that is not reflected in the TDC temperature, which suggests that other temperature-dependent detector components may also be involved.

The comparatively large change in the shift and stretch of the detector in response to the increase in operating temperature at day 85 shows that the stretch responds more quickly to such changes, but takes longer to achieve a new equilibrium. This is consistent with the notion that the stretch is largely controlled by changes in the anode temperature, while the shift is dominated by the temperature of the electronics.¹⁵ Since the anode temperature is dominated by the metal backplate of the detector, its response to changes is more immediate, but takes longer to equilibrate owing to its longer thermal time constant.

On-orbit stim lamp exposures have also been used to monitor the stability of the detector. These images have been taken at a variety of pointing angles and temperatures, and are currently being scheduled every 6 to 8 weeks. They typically contain 5 counts per pixel, which is sufficient to determine the positions of dead spots (see Figure 9) reliably. These positions are being used to track overall detector stability, both by corroborating the changes in the x (dispersion) direction measured by the stim pulses, and, more importantly, by monitoring the stretches in the y dimension. The stim pulses have insufficient baseline in y to provide information about such stretches. No long-term trends have been detected to date.

4.6. Flat Fields

From the outset it was known that stim lamp exposures obtained on orbit would not provide scientifically useful flat field images, because their signal-to-noise ratio would be quite low or, alternately, the exposure time prohibitively long. Furthermore, on-orbit images of the stim lamp would be compromised by the shadows of the grid wires. Consequently, the prelaunch flat field strategy was based on a series of 7 deep stim lamp images taken over an 18 hour interval during integration and test of the spectrograph at the University of Colorado.

For these exposures, MgF_2 diffusers were placed immediately in front of each detector in order to fill in the grid wire shadows. When summed together, the resultant images contained between 42 and 103 counts per pixel on average, depending on the detector segment. Figure 9 shows some of the prominent features of these ground flats, which include dead zones due to blocked pores, hexagonal patterns due to compression along the multi-fiber bundles of the microchannel plate, and brush strokes. Some regions of segments 1B and 2B also exhibited a pronounced moiré pattern that is characterized by a period of 8-9 pixels in the x- direction.

Unfortunately, deep exposures of astronomical sources have shown that the moiré pattern is present in all segments with a significantly greater amplitude in orbital data than in the ground flats. These differences are thought to be artifacts of the conditions under which the ground flats were taken. In particular, the lack of thermal stability evidently introduced

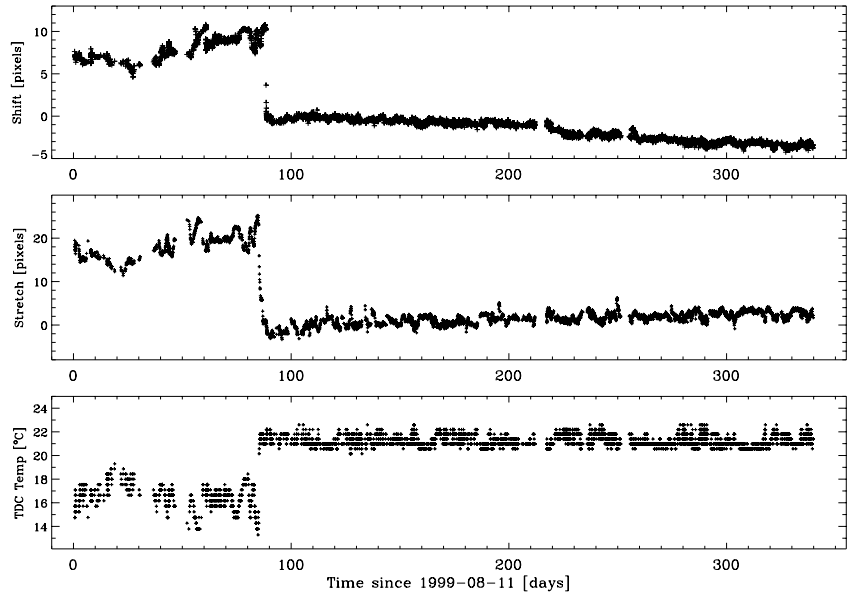


Figure 8 Stability of the pixel coordinate system, as a function of time since launch, for segment 1B. Top: shift in the mean x position of the stim pulses. Middle: stretch in the x scale. Bottom: TDC temperature. The temperature of the spectrograph cavity was changed on day 85. Since that time, both the shift and stretch have been relatively stable.

image motion during an exposure, which resulted in much of the fine-scale structure being washed out. As a result, versions of the ground flats that have been aligned to the orbital reference frame do not removed fixed pattern noise from science data adequately.

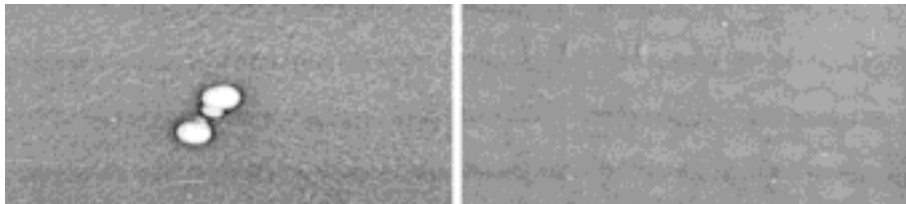


Figure 9 Two regions of the ground flat for segment 1A, shown with an inverted color table. A cluster of large dead spots is evident in the image on the left; smaller dead zones and the hexagonal "chicken wire" pattern are visible in the image on the right.

Instead, a substantially modified flat-fielding strategy is currently being developed. In contrast to the full-image approach, the new strategy uses a high quality, one-dimensional flat field appropriate

to the sum of the pixels illuminated by each aperture. This information is being derived from high signal-to-noise observations (i.e., between 50 and 100) of FUV-bright white dwarfs by means of a "fixed-pattern split" (FP-SPLIT) technique.¹⁶ These one-dimensional flat fields will be applied to science data taken through the same aperture to mitigate fixed-pattern noise. The first observations for this program were taken in mid-July; work is underway to derive flat field information from them. At present, the science data pipeline skips the flat field calibration step altogether.

4.7. Gain

After nearly one year of collecting data, we have noticed a slight drop in the modal gain of the detectors, but it is still a relatively small effect. As the mission progresses and more charge is removed from the MCPs, the high voltage will be adjusted appropriately in order to maintain an adequate gain for proper detector operation. Even with a small drop in gain, the narrow pulse height distributions (50 - 60% of modal gain), which are well separated from zero, prevent a loss of throughput.

The onboard pulse height thresholds are currently set to accept essentially all photons. However, the science data pipeline allows different thresholds to be used in ground processing in order to lower the background for observations where this is important. Although this option is not available in HIST mode (since the pulse height is not saved), the background is much less important for the high count rate observations.

4.8. Background

The detector background rate was measured on the ground during integration and test. This number, which is a combination of the intrinsic detector background (due primarily to radioactive decay of elements in the glass) and cosmic rays,¹⁷ was 2 -3 events per second per segment, with a slight segment-to-segment variation. No hot spots are visible on any segment. This rate was so low that very little spatial variation could be measured, except at the edges of the MCPS, where the rate was slightly higher.

On orbit, the requirement was a rate of <10 cps per segment, which is low enough to ensure that the faintest FUSE targets can be observed. Because the detectors are always viewing the sky and there is no shutter, it is not possible to obtain a truly dark exposure on orbit. Even when not pointing at an astronomical target, airglow lines from the earth's

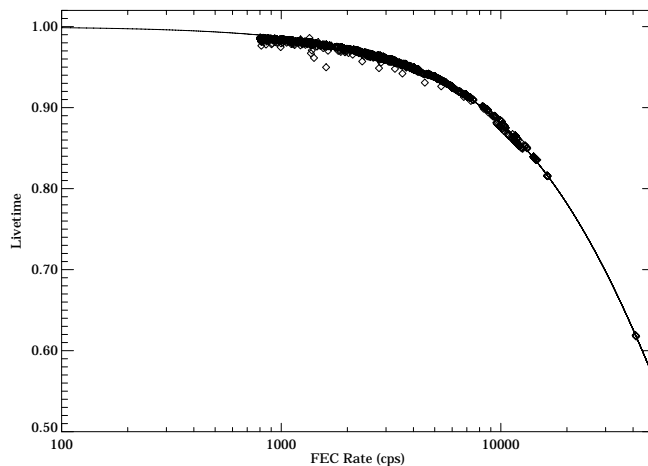


Figure 10 Measured live time (1 - dead time) for segment 2A, as measured in flight. The measured points follow the predicted functional form predicted. The points at low values of the FEC are not plotted because they are incorrectly counted by the DEC.

geocorona fall on the detector at the same location as other spectra do. In addition, scattered light adds a diffuse background over the entire segment. Due to the complication of the airglow lines, the background can only be measured away from the locations of the spectra. Measurements show that this is as low as 5 cps per segment at night, but is typically ~8 cps per segment during the day, implying that difference is due to scattered light. Applying tight pulse height thresholds as described above can lower these numbers by approximately one-half.

4.9. Quantum Detection Efficiency

Since we expect the optical coatings of the FUSE instrument to degrade with time, it is not possible to determine the change in quantum efficiency as a function of time on orbit. The instrument overall has shown a lower than expected decrease in throughput of ~5% during the first year, but this number is highly uncertain; some of this loss is likely due to degradation of the photocathode. The stim lamps do illuminate the detectors directly, but their stability is not known well enough to provide an estimate of QDE variation. A measure of the QDE improvement due to the QDE grid was made, however. Turning the QDE grid off resulted in a 30% loss of throughput, consistent with preflight expectations.

4.10. Dead Time

FUSE was designed to observe faint objects, which typically have count rates of less than several thousand per second. As a result, the electronics were not optimized for high count rates. The dead time at high count rates is thus relatively unimportant, as long as it is known accurately. An analysis of the DPU input state machine architecture, combined with measurements on the flight spare detector enabled an accurate estimate of the functional form of the dead time.¹⁸ Figure 10 shows the dead time measured on orbit for segment 2A (the other segments are similar), as determined by measuring the FEC to DEC ratio; the agreement between the calculated and measured numbers is excellent. No data is shown on the curve at low values of the FEC, since low gain events (such as background events, which dominate at the lowest count rate observations) are incorrectly counted by the DEC, giving an artificially low value. The curve through the points has the expected functional form at high rates, and can thus be extrapolated to the lower rates. The science data pipeline uses the measured FEC rate for each exposure, along with the measured dead time curve equation, to calculate the correct absolute flux.

At count rates >40,000 cps on all four segments, the IDS is unable to keep up with the incoming data stream, and additional losses occur.

4.11. SAA mapping

Although the detector high voltage is lowered to a safe 'SAA level' before each SAA passage, there are still enough counts in the tail of the pulse height distribution to result in count rates of more than 10,000 cps, depending on segment, when passing through the SAA. The gain of these events is low enough that it is not expected to adversely affect the lifetime of the MCPs. Due to orbital precession, the detectors sample a different part of the SAA on every orbit, resulting in the ability to map the particles in the SAA. As expected, the location of the SAA peak corresponds to the location of the maximum occurrences of SEUs. This mapping, combined with several days of exposures in which we modified our SAA contours in order to slightly encroach on the high particle region, will allow us to refine our SAA model, in order to improve the observing efficiency without shortening the life of the detector.

4.12. The "Worm"

An unusual optical anomaly appears in many spectra, due to the interaction between the QDE grid and the astigmatism of the system. Because of this astigmatism, there are two spatially separated foci at most wavelengths. At some wavelengths, one of these foci is ~6 mm in front of the MCPs, which is at the location of the QDE grid. If that focus intercepts a horizontal grid wire, up to 50% of the light can be blocked, rather than the average value of only 5%. Moving the spectra perpendicular to the dispersion direction has a dramatic effect on the severity of the worm. Now that this problem is understood, observing strategies will be developed to minimize it.

5. SUMMARY

The FUSE detectors have been operational on orbit for approximately one year at the time of this writing, and all four segments are performing well. Successful mitigation strategies have been developed for the anomalies discovered early in the mission, such as the regular SEUs. The following table summarizes some of the important characteristics of the FUSE detectors.

Wavelength Coverage	905 – 1187 Å
Active Area	2 segments, each 85 × 10 mm, with a 7 mm gap
Curvature	826 ± 0.025 mm
Pixels	16384 × 1024, ~6 μm (x), 10 – 17 μm (y)
Resolution	20 – 25 μm (x), 80 - 100 μm (y)
QDE	15 – 35%
Dead Time	20% at ~18,000 cps
Background	< 10 cps on orbit per segment
System Power	41.5 w
System Mass	31.1 kg

ACKNOWLEDGEMENTS

We thank the many people at the University of California, Berkeley who contributed to the design, construction, and testing of the FUSE detectors. This work is based on data obtained by the NASA-CNES-CSA FUSE mission operated by the Johns Hopkins University. Financial support to U. S. participants has been provided by NASA contract NAS5-32985.

REFERENCES

- ¹ H. W. Moos et al., “Overview of the Far Ultraviolet Spectroscopic Explorer Mission,” *ApJ* **538**, pp. L1-L6, 2000.
- ² O. H. W. Siegmund, M. Gummin, G. Gaines, G. Naletto, J. Stock, R. Raffanti, J. Hull, R. Abiad, T. Rodriguez-Bell, T. Magoncelli, P. Jelinsky, W. Donakowski, and K. Kromer, “Performance of the double delay line microchannel plate detectors for the Far Ultraviolet Spectroscopic Explorer,” *Proc. SPIE* **3114**, pp. 283-294, 1997.
- ³ D. J. Sahnou, S. D. Friedman, W. R. Oegerle, H. W. Moos, J. C. Green, and O. H. W. Siegmund, “Design and predicted performance of the Far Ultraviolet Spectroscopic Explorer (FUSE),” *Proc. SPIE* **2807**, pp. 2-10, 1996.
- ⁴ O. H. W. Siegmund, R. F. Malina, K. Coburn, and D. Werthimer, “Microchannel Plate EUV Detectors for the Extreme Ultraviolet Explorer,” *IEEE Trans. Nucl. Sci.*, **NS-31**, pp. 776-779, 1984.
- ⁵ M. Hurwitz and S. Bowyer, “The Berkeley EUV spectrometer for the *ORFEUS* mission,” in *Extreme Ultraviolet Astronomy*, R. F. Malina and S. Bowyer (eds), pp. 442-447, Pergamon Press, New York, 1991.
- ⁶ O. H. W. Siegmund et al., “Delay line detectors for the UVCS and SUMER instruments on the SOHO satellite,” *Proc. SPIE* **2280**, 89-100, 1994.
- ⁷ J. B. McPhate, O. H. W. Siegmund, G. A. Gaines, J. V. Vallergera, D. L. Buzasi, and J. S. Hull, “FUV detector system for the Cosmic Origins Spectrograph,” *Proc. SPIE* **4139**, 2000.
- ⁸ D. J. Sahnou et al., “The Far Ultraviolet Spectroscopic Explorer: 1 year in orbit,” *Proc. SPIE* **4139**, 2000.
- ⁹ A. S. Tremsin, O. H. W. Siegmund, M. A. Gummin, P. M. Jelinsky, and J. M. Stock, “Electronic and optical moiré interference with microchannel plates: artifacts and benefits,” *Appl. Opt.* **38**, pp. 2240-2248, 1999.
- ¹⁰ S. J. Conard, R. H. Barkhouser, J. P. Evans, S. D. Friedman, J. W. Kruk, H. W. Moos, R. G. Ohl, and D. J. Sahnou., “The *Far Ultraviolet Spectroscopic Explorer* optical system: lessons learned,” *Proc. SPIE* **4139**, 2000.
- ¹¹ A. N. Cha, D. J. Sahnou, and H. W. Moos, “Processing and interpretation of pre-flight FUSE spectra,” *Proc. SPIE* **3765**, pp. 495-505, 1999.
- ¹² J. B. McPhate, J. V. Vallergera, and G. A. Gaines, “Analysis of FUSE stim PSF variation with count rate,” FUSE-990412-JBM, UCB internal memorandum, 1999.
- ¹³ A. Kenter et al., “In-flight performance and calibration of the Chandra high resolution camera imager,” *Proc. SPIE* **4012**, 2000.
- ¹⁴ D. Roussel-Dupré, J. J. Bloch, E. M. Johnson, and J. Theiler, “ALEXIS; the six year telescope flight experience,” *Proc. SPIE* **3765**, pp. 312-328, 1999.
- ¹⁵ G. A. Gaines, “FUSE Detector Image Stability vs. Temperature,” FUSE-UCB-014, UCB internal memorandum, 1998.

¹⁶ J. A. Cardelli, J. A. and D. C. Ebbets, in *Calibrating Hubble Space Telescope: Proceedings of a Workshop held at STScI*, ed. J. C. Blades & S. J. Osmer (Baltimore, STScI), p. 322, 1994.

¹⁷ O. H. W. Siegmund, J. Vallerger, and M. Lampton, "Background events in microchannel plates," *IEEE Trans. Nucl. Sci.*, **NS-35**, pp. 524-528, 1988.

¹⁸ J. V. Vallerger, J. B. McPhate, and D. Sfeir, "Analysis of Livetime of FUSE detector Electronics," FUSE-981013-JV internal memorandum, 1998.